Effect of Halide-Modified Model Carbon Supports on Catalyst Stability

Kevin N. Wood,[†] Svitlana Pylypenko,[†,‡] Tim S. Olson,[‡] Arrelaine A. Dameron,[‡] Kevin O'Neill,[‡] Steven T. Christensen,[‡] Huyen N. Dinh,[‡] Thomas Gennett,[‡] and Ryan O'Hayre*,[†]

[†]Department of Metallurgical & Materials Engineering, Colorado School of Mines, 1500 Illinois Street, Golden, Colorado 80401, United States

[‡]National Renewable Energy Laboratory, 1617 Cole Boulevard, Golden, Colorado 80401, United States

Ⓢ *Supporting Information*

ABSTRACT: Modification of physiochemical and structural properties of carbon-based materials through targeted functionalization is a useful way to improve the properties and performance of such catalyst materials. This work explores the incorporation of dopants, including nitrogen, iodine, and fluorine, into the carbon structure of highly-oriented pyrolytic graphite (HOPG) and its potential benefits on the stability of PtRu catalyst nanoparticles. Evaluation of the changes in the catalyst nanoparticle coverage and size as a function of implantation parameters reveals that carbon

CATALYST STABILITY
| Poor Durability | Moderate Durability | Excellent Durability |
| *unmodified* | *N-modified* | *N-and F-modified* |

supports functionalized with a combination of nitrogen and fluorine provide the most beneficial interactions, resulting in suppressed particle coarsening and dissolution. Benefits of a carefully tuned support system modified with fluorine and nitrogen surpass those obtained with nitrogen (no fluorine) modification. Ion implantation of iodine into HOPG results in a consistent amount of structural damage to the carbon matrix, regardless of dose. For this modification, improvements in stability are similar to nitrogen modification; however, the benefit is only observed at higher dose conditions. This indicates that a mechanism different than the one associated with nitrogen may be responsible for the improved durability.

KEYWORDS: *electrocatalyst, durability, direct methanol fuel cell, nitrogen, fluorine and iodine functionalization, carbon support*
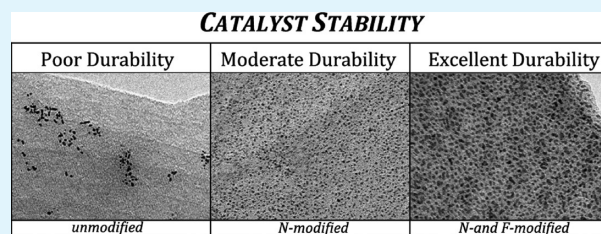
■ INTRODUCTION

Despite significant advances, stability remains one of the most important challenges preventing the widespread commercialization of proton-exchange membrane fuel cells (PEMFCs).[1,2] The degradation of Pt-based electrocatalysts and their supports has a significant impact on the reliability and total lifetime cost of the fuel cell.[3] As such, there is rapidly growing interest in investigating performance degradation of PEMFCs and their material components.[4,5,7,11,12]

Several research groups have suggested that carbon-based catalyst supports can be chemically modified with heteroatoms to create enhanced catalyst–support interactions, thereby substantially improving catalytic activity and stability.[5–27] Almost two decades ago, Shukla et al.[7] demonstrated carbon support functionalization effects for the methanol oxidation reaction (MOR). Within the last five years, heteroatom dopants such as nitrogen, boron, sulfur, and phosphorus have been shown to effectively modify the physical, chemical, and electronic properties of bulk carbon materials.[9–17] While many fabrication methods integrate heteroatom modification into the carbon support synthesis,[8,14,16,18–20] ion implantation could prove to be an important post-synthesis alternative, because of its widespread use (familiarity and accessibility) and the fact that it allows for modification of current commercial catalyst supports.[10] Carbon supports modified by nitrogen

functionalization are the most widely studied, and significant improvements in metal nanoparticle dispersion, durability, and catalytic activity have been demonstrated.[7,11,12,21–27] These improvements are evident for both the oxygen reduction reaction (ORR) and the MOR. Nitrogen-modified carbon supports have been shown to contain a variety of nitrogen functionalities, including graphitic, pyridinic, pyrrolic, and quaternary.[25] While some groups have even hypothesized that nitrogen/carbon moieties are, themselves, active centers for the catalytic reaction,[28] the role of specific moieties in the enhancement of the binding between the catalyst and the support is still a focus of considerable discussion. Recent density functional theory (DFT) studies suggest that the effects of nitrogen on the stability of Pt and PtRu can be either beneficial or detrimental, depending on the specific nitrogen functionality introduced, and for the best beneficial effects, it is likely necessary to have a balance of graphitic, pyridinic, and pyrrolic functionalities.[29]

It has been proposed that edge defects and surface roughness generated by the implantation process could be partially responsible for the improved durability on heteroatom-

functionalized supports. However, it has been shown that implantation of HOPG with inert gases such as argon, which do not incorporate into the matrix, create defects that lead to detrimental effects on support stability.[26,31,32] Similarly, low dosage levels of nitrogen introduced into HOPG have been observed to have negative effects on catalyst durability. This was attributed to the substantial physical damage and small amount of nitrogen functionalization. Increasing the implantation dosage allowed for chemical incorporation of larger amounts of nitrogen (5%–10%) and caused the formation of single-site and clustered multisite nitrogen defects.[24,25] The clusters of nitrogen defects are proposed to be more effective than isolated defects at stabilizing metal nanoparticles and preventing migration/coalescence of the metal phase.[25] Recently, ion implantation has also been used to functionalize commercially available carbon powders.[29–32,37]

This study focuses on the modification of the model HOPG substrates through the ion implantation of halides, specifically fluorine and iodine. Raman spectroscopy and X-ray photoelectron spectroscopy (XPS) were used to determine the structural and chemical modifications of the HOPG substrates as a function of dopant and implantation conditions. Through the use of magnetron-sputtering-based deposition, we were able to produce consistent, reproducible, non-preferential Pt–Ru catalyst coverages, which were subsequently subjected to electrochemical durability cycling. Transmission electron microscopy (TEM) was used to evaluate the changes in the coverage and particle size distribution before and after cycling, and correlate them with specific structural effects and chemical functionalities associated with the different modifications. This work demonstrates that incorporation of iodine, fluorine, and nitrogen into the graphitic structure of HOPG modifies the substrate surface chemistry and changes catalyst–substrate interactions. In iodine-modified samples, improved durability is most likely associated with the presence of polyiodide species. The improved durability observed with fluorine modification is co-dependent on the presence of nitrogen. In this co-implanted system, it is hypothesized that the enhanced durability is due to (1) the charge difference between nitrogen and carbon, (2) nitrogen's incorporation into the carbon ring structure, and (3) the electron-withdrawing nature associated with the formation of C–F bonds.

■ EXPERIMENTAL SECTION

Highly oriented pyrolytic graphite (HOPG, grade 2, 10 mm × 10 mm × 1 mm, SPI, Inc.) was used as the model carbon substrate material. Ion implantation of HOPG substrates was performed with a 3-cm direct current (DC) (ITI) ion source (Veeco) at room temperature, using an ion beam of N_2, I_2, CF_4, or a mix of N_2 and CF_4 directed to the surface at an incident angle of 35°. CF_4 was chosen instead of fluorine gas, because of its relatively benign nature. For all precursors, the ion beam energy was kept constant at 100 eV, and the ion current and the time of implantation were in the range of 13–42 mA and 45–120 s, respectively. These conditions correlate to an estimated ion dosage in the ranges of 10^{16}–10^{17} ions/cm². Sample dosages and conditions are shown in Table 1 in the Supporting Information. It was observed that the chemical nature and surface concentration of the inherent nitrogen heteroatoms varied with the CF_4 implantation parameters. The CF_4 process gas did not contain nitrogen, as was determined by mass spectroscopy.

Raman spectra were collected using a Nd:YAG laser with an excitation wavelength of 532 nm, in conjunction with a double-grating UHTS300 spectrometer set to the 600 g/mm option with a center wavelength of 598 nm. The setup also included a 100× Nikon objective lens and an Andor iDus CCD camera. Each single Raman

spectrum resulted from 25 scans, with each scan having an integration time of 0.5 s. The D/G ratio was calculated by subtracting the background from both peak intensities and then dividing the D band (defect) peak intensity by the G band (graphitic carbon) peak intensity. X-ray photoelectron spectroscopy (XPS) survey and high-resolution spectra were collected on a Kratos Nova XPS instrument, using a monochromatic Al Kα source operated at 300 W. Data analysis was performed using CasaXPS software and included subtraction of the linear background and charge referencing, using the graphitic peak at 284.6 eV.

$Pt_{1−x} Ru_x$ nanoparticles were sputtered onto the modified and unmodified HOPG substrates from a single composition $Pt_{0.5} Ru_{0.5}$ (ACI Alloys) alloyed target with a 2-in. Onyx magnetron sputter gun (Angstrom Sciences). DC magnetron sputtering was performed using an MDX 1.5 kW DC power supply (Advanced Energy). The samples were positioned at a distance of 1.5 in. directly above the target, and the deposition was done after establishing a base pressure below 4×10^{-6} Torr. Nanoparticles were deposited by sputtering for 5 s in an inert argon environment at a constant power of 20 W and a constant pressure of 20 mTorr Ar. Material flux was limited to very short time frames (few seconds) by the use of a shutter between the sample and the source.

After sputtering deposition, electrochemical cycling of HOPG substrates was performed using the three-electrode configuration. In a special aqueous cell, the HOPG acted as the working electrode, while Ag/AgCl was used for the reference electrode and a Pt wire counter electrode completed the circuit. The modified HOPG substrates were cycled this way 300 times in 1 M H_2SO_4/1 M MeOH from 0 to 1.2 V vs. Ag/AgCl at 250 mV/s.

TEM images the Pt–Ru nanoparticles on HOPG substrates were obtained using a Philips CM200 TEM microscope. The samples were prepared by peeling off a thin surface layer of the HOPG sample and positioning it between the two grids of a Cu double grid (Electron Microscopy Sciences). Evaluation of the coverage and particle size analysis was conducted using Photoshop and Igor, following methods that have been reported elsewhere.[9,25,26] The coverage was determined by applying both high pass and threshold filters to separate the background HOPG from the Pt–Ru particles. These particles were then analyzed by converting black Pt–Ru particles to a ratio versus total area of the image. A representative number of single nanoparticles were then measured to obtain average particle size. This allowed for size resolution down to ~0.1 nm.

■ RESULTS AND DISCUSSION

The relationship between the chemical and structural effects caused by ion implantation to the stability of overlying PtRu catalyst nanoparticles supported on HOPG substrates was established through TEM analysis of catalyst coverage and particle size variations. First, results were obtained for the two reference samples, unmodified and N-modified HOPG, shown in Figure 1. Initial TEM images show the substrates to have consistent PtRu particle size and coverage (see Figures 1a and 1c). For the post-cycled, unmodified sample (Figure 1b), poor coverage and larger particle size were observed, indicating degradation of the catalyst through dissolution and migration/coalescence of the metal phase. However, doping the carbon support with nitrogen at a dosage of 10^{16} ions/cm² (Figure 1d) resulted in better coverage retention and smaller changes in the particle sizes. These findings are consistent with the previous reports for unmodified and nitrogen-modified HOPG and will be used to compare the stability of PtRu nanoparticles on iodine- and fluorine-modified HOPG samples.[29]

Support Modification with Iodine. Figure 2 compares the Raman spectra of iodine-modified HOPG at two dosages to the spectra acquired for the unmodified and nitrogen-modified reference samples. The major change in the Raman spectra associated with implantation is the appearance of a defect peak
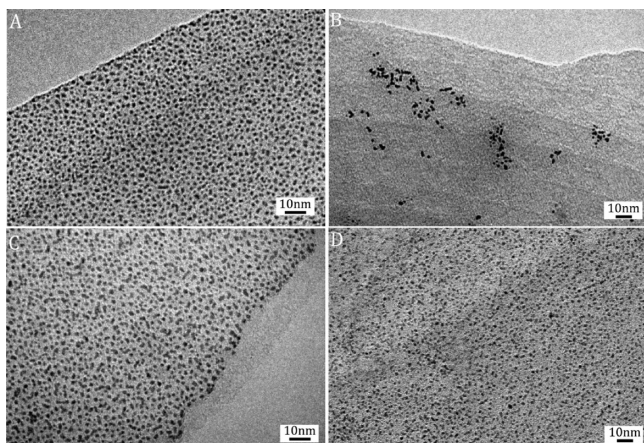
6729

dx.doi.org/10.1021/am301898e | ACS Appl. Mater. Interfaces 2012, 4, 6728–6734

Figure 1. Transmission electron microscopy (TEM) images of pre-cycle and post-cycle unmodified and nitrogen-modified samples: (A) unmodified, pre-cycled, (B) unmodified, post-cycled, (C) N-modified, pre-cycled, and (D) N-modified, post-cycled.

Figure 3. TEM images of pre- and post-cycled low and high-dose iodine-modified samples: (A) low-dose iodine-modified, pre-cycled; (B) low-dose iodine-modified, post-cycled; (C) high-dose iodine-modified, pre-cycled; and (D) high-dose iodine-modified, post-cycled.

(D-band) near 1350 cm^{-1}. In the iodine sample modified with 10^{16} ions/cm^2 (low dose), the spectrum reveals the presence of this defect peak, but no response in the range expected for polyiodide species (100-200 cm^{-1}).[35,36] This suggests that low-dose implantation of iodine creates structural damage to the carbon, but does not provide sufficient driving force to create extended iodine structures. In the sample modified by 10^{17} ions/cm^2 (high-dose), the intensity of the D-band remains fairly consistent with that of the low-dose sample, but the appearance of an iodine resonance peak at ~170 cm^{-1} was observed. The lack of further change to the D-band indicates that structural damage to the carbon did not increase with dose. However, the appearance of an iodine resonance peak suggests the incorporation of iodine into the support material.[33,34] XPS analysis also suggested the presence of polyiodide species at binding energies of ~619 and 620 eV (see Figure 1a in the Supporting Information).[35]

For the iodine-modified samples (Figure 3), the pre-cycled catalyst morphology is consistent with the previous samples shown in Figure 1. TEM images of the post-cycled low-dose iodine-modified sample (Figure 3b) suggest a significant loss of catalyst coverage, which is indicative of poor stability (Figure
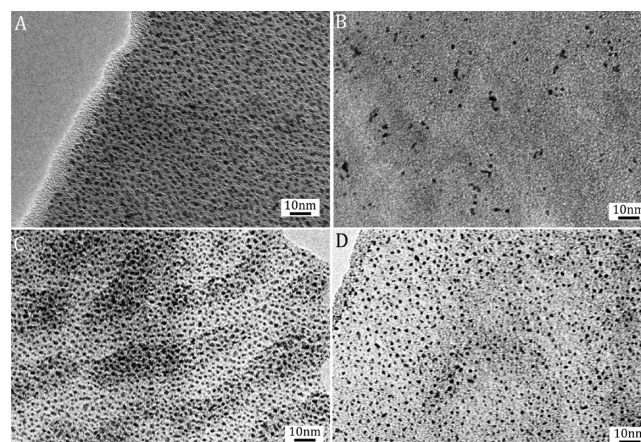
3b). In particular, the formation of large agglomerates on this sample is strong evidence of insufficient modification to improve catalyst stability on the surface, even though the durability of this low-dosage iodine-modified sample showed slight improvement over the unmodified baseline (see Figure 1b in the Supporting Information). Figures 3c and 3d show TEM micrographs for the pre- and post-cycled high-dose iodine-modified sample, the analysis of which shows ~40% retention in particle coverage and an ~0.4 nm decrease in particle size.[25] These results are a significant improvement over the unmodified sample, and are almost equivalent to the beneficial effect observed for nitrogen-modified samples. Significant improvement in durability of the high-dose iodine-modified sample, compared to the low-dose iodine-modified sample, is most likely related to the formation of polyiodide species. Polyiodide species have shown to have beneficial effects on catalytic activity of the carbon-based materials used in batteries.[35]

Support Modification with Fluorine. Figure 4 compares the Raman spectra of HOPG modified with fluorine at two dosages, versus the spectra acquired for the unmodified and nitrogen-modified reference samples. These data show very
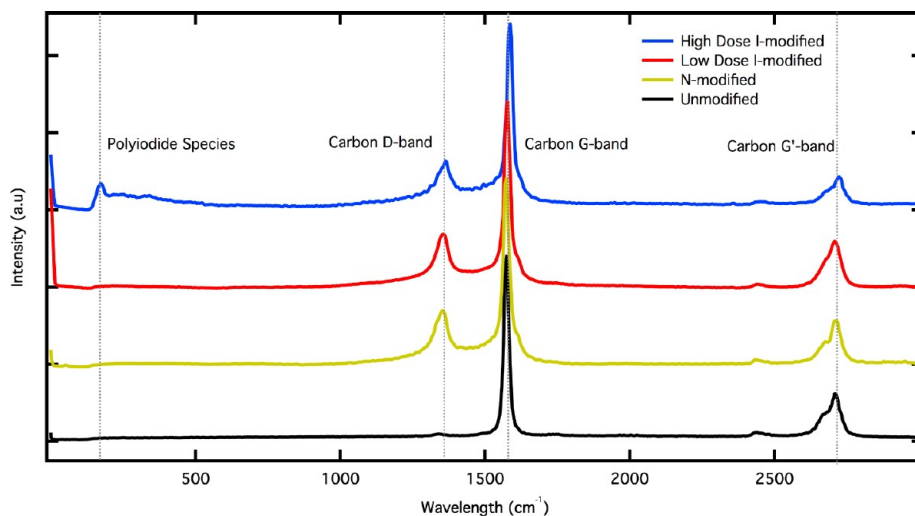

Figure 2. Raman spectra of iodine-modified HOPG samples, compared to unmodified and nitrogen-modified reference samples.
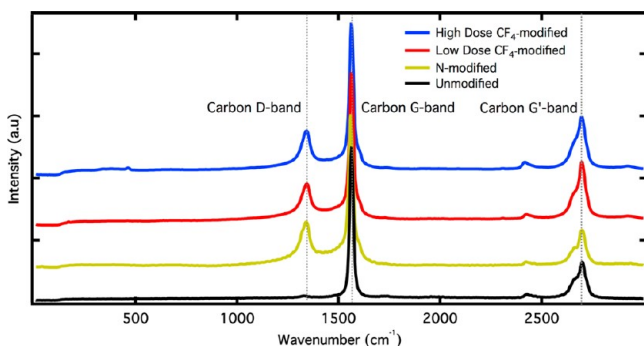
Figure 4. Raman spectra of CF$_4$-modified HOPG samples, compared to unmodified and nitrogen-modified reference samples.

Figure 6. TEM images of the pre- and post-cycled low-dose and high-dose CF$_4$-modified samples: (A) low-dose, pre-cycled; (B) low-dose, post-cycled; (C) high-dose, pre-cycled; and (D) high-dose, post-cycled.

small changes in the C defect peak for the CF$_4$-modified samples, compared against the nitrogen-modified reference, indicating that there are few structural differences between the nitrogen-modified sample and the CF$_4$-modified samples at either dose.

Figure 5 shows XPS spectra for both CF$_4$-modified samples against unmodified and nitrogen-modified reference samples. These spectra illustrate significant differences between the nitrogen-modified and high-dose CF$_4$-modified sample resulting from the incorporation of fluorine. The incorporation of fluorine into graphitic carbon is supported by observations of C−F species at BE = 288−290 eV, and C*−C−F species at BE = 285−286 eV. Equally significant is the fact that peaks above BE 291 eV, which correspond to fragmented precursor species such as CF$_3$ and CF$_2$, are not observed. In addition, along with fluorine incorporation, CF$_4$-modified samples also showed a significant incorporation of nitrogen. XPS analysis indicated ∼2 at.% and ∼8 at.% nitrogen in the low- and high-dose CF$_4$-modified samples, respectively. The increase in nitrogen concentration and C−N species at 286 eV appears to be dose-dependent.

TEM images for the low- and high-dose CF$_4$-modified pre- and post-cycled samples are shown in Figure 6. The micrograph for the post-cycled lower-dose CF$_4$-modified sample (Figure 6b) shows a significant reduction in the frequency and size of agglomerates, when compared with the unmodified and lower-dose iodine-modified samples, but a substantial loss of catalyst coverage when compared to the nitrogen-modified sample. Similar to the iodine modification, fluorine modification at
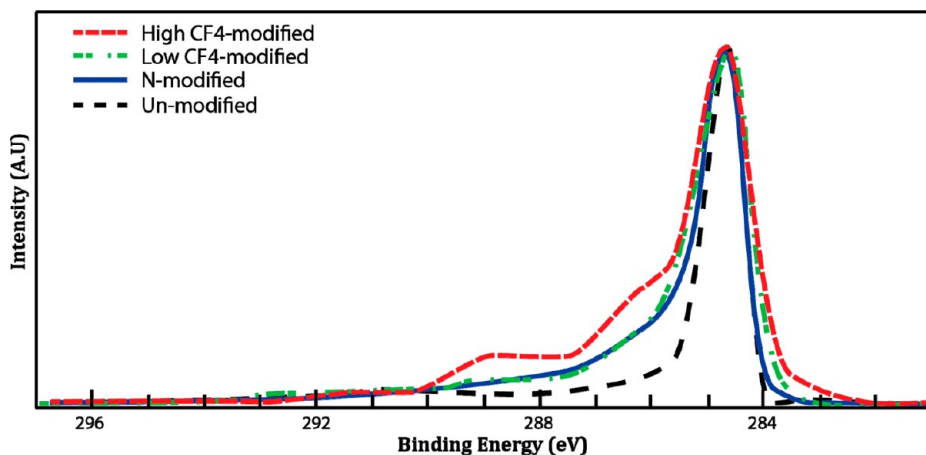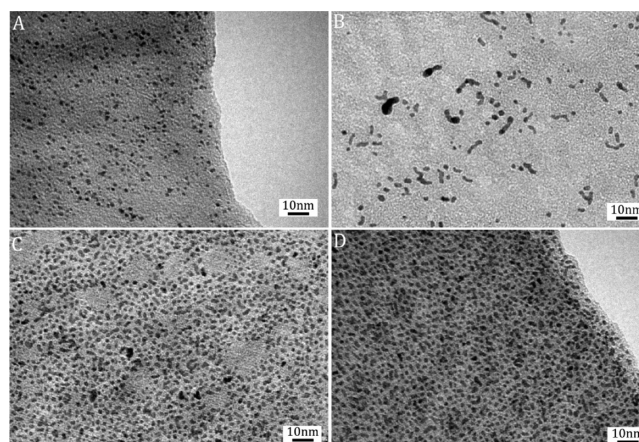
higher dose also yielded an enhancement in durability, as demonstrated by improved retention of both catalyst particle size and coverage (see Figure 6d). These results show that the high-dose CF$_4$-modified sample actually outperforms the nitrogen-modified samples. The best results obtained with optimized nitrogen-modified samples have previously showed an ∼60% reduction in coverage and an ∼0.4 nm decrease in the particle size.[25] By comparison, the presence of fluorine functionalities included with nitrogen moieties showed dramatic improvement over the N-modified results, minimizing coverage loss to ∼20% and retaining the particle size to within ∼0.2 nm of the pre-cycle value.

Support Modification with Fluorine and Nitrogen. In light of the finding that, along with fluorine incorporation, CF$_4$ modification resulted in the incorporation of significant amounts of nitrogen, a further set of experiments utilizing intentional mixing of relative amounts of nitrogen and fluorine precursors (N$_2$ and CF$_4$) was used to understand the relative importance of the contributions from nitrogen versus fluorine on the catalyst stability. Figure 7a shows the elemental composition of a series of HOPG samples functionalized with fluorine and nitrogen. For reference, the samples are labeled A−D, where the sample with the most fluorine is labeled as "A" and the sample with the lowest amount of fluorine as "D".

Figure 5. High-resolution C 1s XPS spectra of CF$_4$-modified HOPG samples, compared to unmodified and nitrogen-modified reference samples.
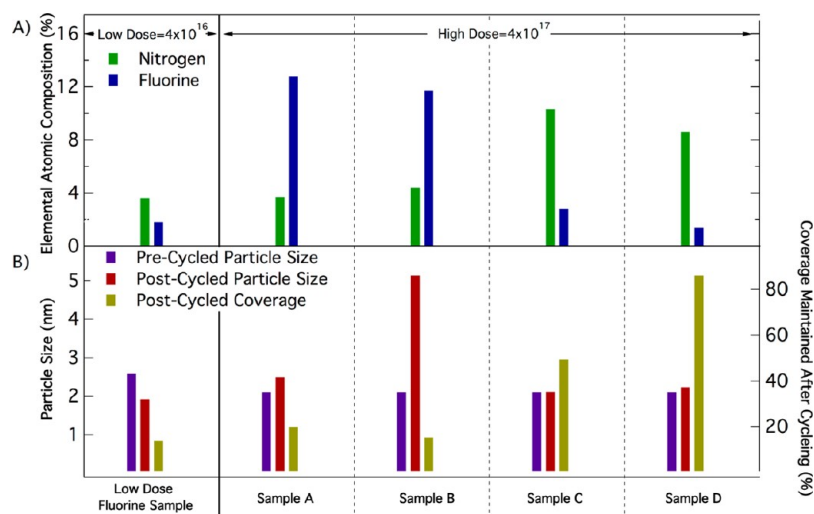
Figure 7. Characterization of co-implanted samples with varying ratios of nitrogen versus fluorine concentrations: (a) XPS elemental composition and (b) average particle size obtained from the analysis of TEM micrographs.
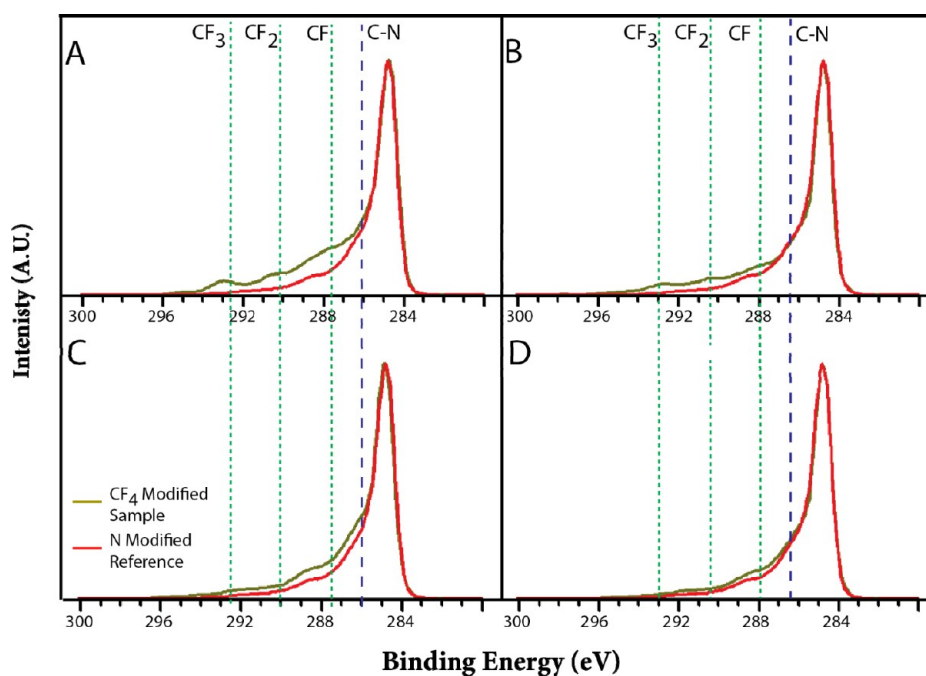

Figure 8. High-resolution C 1s XPS spectra of co-implanted sample (A−D), compared to nitrogen-modified reference sample.

Figure 8 compares C 1s spectra from this set of samples to that of the solely nitrogen-doped reference sample.

Comparing C 1s spectra of co-implanted sample A versus the nitrogen-modified reference sample, we see pronounced peaks at ~288, 290.5, and 293 eV, caused by carbon species bound to one, two and three fluorine atoms, respectively. CF_2 and CF_3 species are most likely fragments of precursor that adsorbed on the surface. Sample B, although containing slightly less fluorine, also exhibits a similar, slightly less-defined shoulder in the BE range of 287−295 eV. This result again indicates associatively adsorbed precursor fragments, but in a smaller concentration than that observed for sample A. Representative TEM images of the post-cycle catalyst morphology for the four co-doped samples are provided in Figure 9. After cycling, samples with the highest fluorine content and lowest nitrogen content (A and B) suffer significant particle coverage loss along with

evidence of particle aggregation. We attribute this poor stability performance to the presence of precursor fragments loosely attached to the surface (associative adsorption).

Sample C (Figure 8) showed a significant decrease in fluorine content (~3 at. %), compared to samples A and B, and an increase in nitrogen content to ~10.5 at. %, which is higher than the nitrogen concentration in the nitrogen-modified reference sample. The C 1s XPS spectrum of sample C shows an increase in the amount of C−N species at BE = 286 eV, when compared with the nitrogen baseline. In addition, we see a significant increase in the amount of species at BE ≈ 288−290 eV, indicating the presence of C−F bonds. TEM micrographs of post-cycled sample C (Figure 9C) reveal inconsistent behavior, where some areas manifest excellent durability (good coverage and consistent particle size) while other areas suffer significant coverage loss (albeit without much change in particle
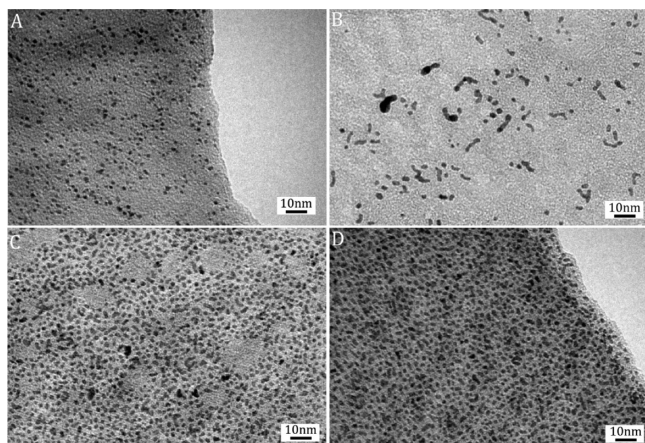
Figure 9. TEM images of post-cycled co-implanted HOPG samples: (A) 13% fluorine, 4% nitrogen; (B) 11.5% fluorine, 4.5% nitrogen; (C) 3% fluorine, 10.5% nitrogen; and (D) 1.5% fluorine, 8.5% nitrogen.

size or particle morphology). Sample D shows a chemical composition closest to the previously discussed high-dose CF_4-modified sample: ~8.5 at. % nitrogen and ~1.5 at. % fluorine. Comparing the C 1s XPS spectrum to that of the best performing nitrogen-modified sample, we see a slight increase in C−F species (~288 eV) and a similar concentration of C−N species (~286 eV). Most notably, however, fragmented precursor species, such as CF_2 and CF_3, are not observed. Analysis of the TEM micrograph of the post-cycled sample D (Figure 9D) confirms that elimination of the precursor fragments associatively bonded to the surface, while still providing direct incorporation of fluorine and nitrogen functionalities into the graphitic network. A comparison of Figure 9D with Figure 1D clearly reveals that the improved coverage and particle stability of this co-doped sample surpasses the positive effects of nitrogen doping by itself.

Nitrogen dopants in carbon have been shown to have an electron-withdrawing nature that is hypothesized to improve the strength of metal carbon interactions and act as a trapping state that helps to prevent catalyst migration.[25,33] It is most likely that the role of nitrogen in the co-implanted systems is same as in nitrogen-implanted systems. Fluorine cannot be directly incorporated into the ring structure of the carbon support and, therefore, cannot act as a trapping site. However, the addition of fluorine to the support may stabilize the catalyst particle size by decreasing the dissolution of the metal phase more significantly than by nitrogen modification alone, because of the strong electronegative character of fluorine. Complicating the incorporation of active fluorine species into the catalyst support system is the fact that high precursor concentrations of CF_4 are difficult to completely ionize, leading to large amounts of associative bonding and catalyst detachment (as observed in our highly concentrated fluorine samples). However, the combined fluorine/nitrogen studies suggest that if the correct ratio of nitrogen and fluorine is incorporated into the support, associatively bound carbon- and fluorine-containing precursor species can be eliminated, and the resulting catalyst stabilization effects are significant.

CONCLUSIONS

The results shown above demonstrate the potential to tune catalyst/support interactions using chemically modified support structures. It was shown that iodine modification improves catalyst durability, compared to unmodified structures. This improvement was associated with the presence of polyiodide species, and minimal C−I interactions. In the nitrogen/fluorine system, both C−F and C−N bonds are formed, the electronic properties of fluorine improve resistance to metal dissolution while the nitrogen sites mitigate migration and coalescence through incorporation into the carbon ring structure. This co-incorporation of nitrogen and fluorine seems to have the potential to improve the interactions between the carbon support and the overlying metal nanoparticles, beyond the effects observed for just nitrogen, as long as the heteroatoms are incorporated into the support and the surface remains free from precursor fragments. The results presented in the work provide a framework for the selection of catalyst/support functionalization and offer new directions for fuel cell electrocatalyst optimization in order to reach DOE targets for durability and reliability.

ASSOCIATED CONTENT

Ⓢ Supporting Information

This material is available free of charge via the Internet at http://pubs.acs.org.

AUTHOR INFORMATION

Corresponding Author

*Tel.: 303-273-3952. E-mail: rohayre@mines.edu.

Notes

The authors declare no competing financial interest.

ACKNOWLEDGMENTS

REFERENCES

(1) Xu, X.; Ye, S. *J. Power Sources* **2007**, *172*, 145.
(2) Borup, R.; Meyers, J.; Pivovar, B.; Kim, Y. S.; Mukundan, R.; Garland, N.; Myers, D.; Wilson, M.; Garzon, F.; Wood, D.; Zelenay, P.; More, K.; Stroh, K.; Zawodzinski, T.; Boncella, J.; McGrath, J. E.; Inaba, M.; Miyatake, K.; Hori, M.; Ota, K.; Ogumi, Z.; Miyata, S.; Nishikata, A.; Siroma, Z.; Uchimoto, Y.; Yasuda, K.; Kimijima, K.-I.; Iwashita, N. *Chem. Rev.* **2007**, *107*, 3904.
(3) Mathias, M.; Gasteiger, H.; Makharia, R.; Kocha, S.; Fuller, T.; Pisco, J. *Abstr. Pap. Am. Chem. Soc.* **2004**, *228*, U653.
(4) Yu, J. R.; Matsuura, T.; Yoshikawa, Y.; Islam, M. N.; Hori, M. *Electrochem. Solid State Lett.* **2005**, *8*, A156.
(5) Yu, J. R.; Matsuura, T.; Yoshikawa, Y.; Islam, M. N.; Hori, M. *Phys. Chem. Chem. Phys.* **2005**, *7*, 373.
(6) Ozaki, J. I.; Anahara, T.; Kimura, N.; Oya, A. *Carbon* **2006**, *44*, 3358−3361.
(7) Shukla, A. K.; Ravikumar, M. K.; Roy, A.; Barman, S. R.; Sarma, D. D.; Arico, A. S.; Antonucci, Y.; Pino, L.; Giordano, N. *J. Electrochem. Soc.* **1994**, *141*, 1517−1522.
(8) Maldonado, S.; Morin, S.; Stevenson, K. J. *Carbon* **2006**, *44*, 1429−1437.

(9) Zhou, Y. K.; Neyerlin, K.; Olson, T. S.; Pylypenko, S.; Bult, J.; Dinh, H. N.; Gennett, T.; Shao, Z. P.; O'Hayre, R. *Energy Environ. Sci.* **2010**, *3*, 1437.

(10) Bangert, U.; Bleloch, A.; Gass, M. H.; Seepujak, A.; vandenBerg, J. *Phys. Rev. B* **2010**, *81*.

(11) Lei, Z. B.; An, L. Z.; Dang, L. Q.; Zhao, M. Y.; Shi, J.Y.; Bai, S. Y.; Cao, Y. D. *Microporous Mesoporous Mater.* **2009**, *119*, 30.

(12) Lei, Z. B.; Zhao, M. Y.; Dang, L. Q.; An, L. Z.; Lu, M.; Lo, A. Y.; Yu, N. Y.; Liu, S. B. *J. Mater. Chem.* **2009**, *19*, 5985.

(13) Li, X. G.; Park, S.; Popov, B. N. *J. Power Sources* **2010**, *195*, 445.

(14) Maldonado, S.; Stevenson, K. J. *J. Phys. Chem. B* **2005**, *109*, 4707.

(15) Pocard, N. L.; Alsmeyer, D. C.; Mccreery, R. L.; Neenan, T. X.; Callstrom, M. R. *J. Mater. Chem.* **1992**, *2*, 771.

(16) Prehn, K.; Warburg, A.; Schilling, T.; Bron, M.; Schulte, K. *Compos. Sci. Technol.* **2009**, *69*, 1570.

(17) Terrones, M.; Redlich, P.; Grobert, N.; Trasobares, S.; Hsu, W. K.; Terrones, H.; Zhu, Y. Q.; Hare, J. P.; Reeves, C. L.; Cheetham, A. K.; Ruhle, M.; Kroto, H. W.; Walton, D. R. M. *Adv. Mater.* **1999**, *11*, 655.

(18) Vijayaraghavan, G.; Stevenson, K. J. *Langmuir* **2007**, *23*, 5279.

(19) Sun, C. L.; Chen, L. C.; Su, M. C.; Hong, L.S.; Chyan, O.; Hsu, C. Y.; Chen, K. H.; Chang, T. F.; Chang, L. *Chem. Mater.* **2005**, *17*, 3749.

(20) Chen, L.C.; Wen, C. Y.; Liang, C. H.; Hong, W. K.; Chen, K. J.; Cheng, H. C.; Shen, C. S.; Wu, C. T.; Chen, K. H. *Adv. Funct. Mater.* **2002**, *12*, 687.

(21) Roy, S. C.; Christensen, P. A.; Hamnett, A.; Thomas, K. M.; Trapp, V. *J. Electrochem. Soc.* **1996**, *143*, 3073.

(22) Maiyalagan, T. *Appl. Catal., B* **2008**, *80*, 286.

(23) Wu, G.; Li, D. Y.; Dai, C. S.; Wang, D. L.; Li, N. *Langmuir* **2008**, *24*, 3566.

(24) Pylypenko, S.; Queen, A.; Olson, T. S.; Dameron, A.; O'Neill, K.; Neyerlin, K. C.; Pivovar, B.; Dinh, H. N.; Ginley, D. S.; Gennett, T.; O'Hayre, R. *J. Phys. Chem. C* **2011**, *115*, 13667−13675.

(25) Pylypenko, S.; Queen, A.; Olson, T. S.; Dameron, A.; O'Neill, K.; Neyerlin, K. C.; Pivovar, B.; Dinh, H. N.; Ginley, D. S.; Gennett, T.; O'Hayre, R. *J. Phys. Chem. C* **2011**, *115*, 13676−13684.

(26) Zhou, Y. K.; Pasquarelli, R.; Holme, T.; Berry, J.; Ginley, D.; O'Hayre, R. *J. Mater. Chem.* **2009**, *19*, 7830.

(27) Ye, S. Y.; Vijh, A. K.; Dao, L. H. *J. Electrochem. Soc.* **1996**, *143*, L7.

(28) Liu, G.; Li, X.; Ganesan, P.; Popov, B. N. *Appl. Catal., B* **2009**, *93* (1−2), 156−165.

(29) Pylypenko, S.; Olson, T.; Dameron, A.; Borisevich, A.; More, K.; Holme, T.; Wood, K. N.; O'Neill, K.; Hurst, K.; Christensen, S.; Ginley, D.; Pivovar, B.; Dinh, H.; Gennett, T.; O'Hayre, R. *ECS Meeting Abstracts* **2011**, *1102* (16), 1191−1191.

(30) Olson, T.; Joghee, P.; Dameron, A.; Corpuz, A.; Pylypenko, S.; Hurst, K.; Ginley, D.; Gennett, T.; O'Hayre, R.; Dinh, H. *ECS Meeting Abstracts* **2011**, *1102* (16), 768−768.

(31) Wood, K. N.; Christensen, S. T.; Pylypenko, S.; Olson, T. S.; Dameron, A. A.; Hurst, K. E.; Dinh, H. N.; Gennett, T.; O'Hayre, R. *MRS Commun.* **2012**, *2* (3), 85−89 (DOI: 10.1557/mrc.2012.13).

(32) Corpuz, A. R.; Olson, T. S.; Joghee, P.; Pylypenko, S.; Dameron, A. A.; Dinh, H. N.; O'Neill, K. J.; Hurst, K. E.; Bender, G.; Gennett, T.; Pivovar, B. S.; Richards, R. M.; O'Hayre, R. P. *J. Power Sources* **2012**, *217* (0), 142−151.

(33) Zhou, Y. K.; Holme, T.; Berry, J.; Ohno, T. R.; Ginley, D.; O'Hayre, R. *J. Phys. Chem. C* **2010**, *114*, 506.

(34) Matter, P. H.; Zhang, L.; Ozkan, U. S. *J. Catal.* **2006**, *239*, 83.

(35) Yao, Z.; Nie, H.; Yang, Z.; Zhou, X.; Liu, Z.; Huang, S. *Chem. Commun.* **2012**, *48*, 1027.

(36) Kalita, G.; Wakita, K.; Takahashi, M.; Umeno, M. *J. Mater Chem.* **2011**, *21*, 15209.

(37) Joghee, P.; Pylypenko, S.; Olson, T.; Dameron, A.; Corpuz, A.; Dinh, H. N.; Wood, K.; O'Neill, K.; Hurst, K.; Bender, G.; Gennett, T.; Pivovar, B.; O'Hayre, R. *J. Electrochem. Soc.* **2012**, *159*, F768.